Polar auxin transport modulates early leaf flattening

Qingqing Wang[a,b,1,2] (iD), Marco Marconi[c,2] (iD), Chunmei Guan[a,2] (iD), Krzysztof Wabnik[c,3] (iD), and Yuling Jiao[a,b,d,e,3] (iD)

The flattened leaf form is an important adaptation for efficient photosynthesis, and the developmental process of flattened leaves has been intensively studied. Classic microsurgery studies in potato and tomato suggest that the shoot apical meristem (SAM) communicates with the leaf primordia to promote leaf blade formation. More recently, it was found that polar auxin transport (PAT) could mediate this communication. However, it is unclear how the expression of leaf patterning genes is tailored by PAT routes originating from SAM. By combining experimental observations and computer model simulations, we show that microsurgical incisions and local inhibition of PAT in tomato interfere with auxin transport toward the leaf margins, reducing auxin response levels and altering the leaf blade shape. Importantly, oval auxin responses result in the bipolar expression of *SlLAM1* that determines leaf blade formation. Furthermore, wounding caused by incisions promotes degradation of SlREV, a known regulator of leaf polarity. Additionally, computer simulations suggest that local auxin biosynthesis in early leaf primordia could remove necessity for external auxin supply originating from SAM, potentially explaining differences between species. Together, our findings establish how PAT near emerging leaf primordia determines spatial auxin patterning and refines *SlLAM1* expression in the leaf margins to guide leaf flattening.

leaf development | auxin | patterning | polar auxin transport | flattening

Plant leaves typically form thin blades to optimize vital processes, such as photosynthesis, transpiration, and respiration (1–3). How leaves form flattened structures has been one of the most intensively studied problems in the plant development. During vegetative growth, the shoot apical meristem (SAM) maintains stem cells and generates leaves from its periphery. Following initiation, leaf primordia develop along three orthogonal axes, namely, the adaxial–abaxial (also called dorsoventral), proximodistal, and mediolateral axes. Flattened leaf blades typically undergo limited adaxial–abaxial growth and prolonged growth along the latter two axes.

Contemporary knowledge of leaf flattening dates back to the pioneering microsurgical experiments of Ian Sussex (4, 5), in which early or incipient leaf primordia developed into axisymmetric structures after they were microsurgically separated from the SAM (6, 7). Based on those results, it has been postulated that a signal moves from the SAM toward incipient leaf primordia to promote adaxial fate, which appears to be important for flattening (8). This signal, now called the Sussex signal, serves as a striking example in which organ patterning requires information from undifferentiated stem cells. Recently, it has been suggested that polar auxin transport (PAT) mediated by PIN-FORMED1 (PIN1) at the epidermal layer mediates the Sussex signal (9). PAT around and within emerging leaf primordia leads to spatial auxin distribution along the adaxial–abaxial axis: the highest auxin levels are in the middle domain, slightly lower levels are in the abaxial domain, and the lowest auxin levels are in the adaxial domain (9–12). The adaxial–abaxial interface establishes before primordium emergence (12), and spatial auxin distribution emerges afterward. In addition to the tangential incisions used in the above experiments, lateral incisions at both sides of an emerging primordium similarly have been shown to lead to axisymmetric structure formation (13, 14).

Extensive molecular genetic studies in Arabidopsis have revealed the presence of a transcriptional regulatory network promoting leaf adaxial–abaxial polarity establishment. The SAM peripheral zone is prepatterned with the adaxial-promoting *ASYMMETRIC LEAF2* (*AS2*) and HD-ZIPIII genes, such as *REVOLUTA* (*REV*), expressed in the center, and abaxial-promoting KANADI (KAN) genes, such as *KAN1*, expressed farther out. Emerging leaf primordia span both domains (12, 15–17). HD-ZIPIII and other adaxial-promoting genes expressed in the adaxial domain suppress *KAN* and other abaxial-promoting genes expressed in the abaxial domain, and vice versa (18), forming the adaxial–abaxial axis. The abovementioned spatial auxin distribution, together with adaxially expressed *MONOPTEROS* (*MP*), which encodes a class-A ARF, activates the expression of the WUSCHEL-RELATED HOMEOBOX (WOX) genes *WOX1* and *PRESSED*

Significance

Flattened leaf blade formation is a key adaption of plants to the environment, but its developmental regulation remains to be resolved. Classical microsurgery experiments suggest that a mobile signal, known as the Sussex signal, in the shoot apex is required for flattened leaf formation. A recent study found that polar auxin transport contributes to the Sussex signal, but how microsurgeries interact with polarity genes remains elusive. Here, we combine live-imaging and computer model simulations to show that an oval-shaped auxin response in inner cells of leaf primordium is essential for the formation of bipolar *SlLAM1* expression domain, which establishes initial bilateral leaf primordia. Microsurgeries lead to an axisymmetric domain shape and can interfere with other polarity factors.

[1]Present address: Staidson (Beijing) Biopharmaceuticals Co., Ltd., Beijing 100176, China.

[2]Q.W., M.M., and C.G. contributed equally to this work.

[3]To whom correspondence may be addressed. Email: k.wabnik@upm.es or yuling.jiao@pku.edu.cn.

FLOWER (*PRS*) in Arabidopsis (11), and *SlLAM1* in tomato (19), in the middle domain that spans the leaf margins, thus defining the mediolateral axis for leaf blade outgrowth. The leaf margins promote bilateral symmetry, which is further maintained and amplified by the microtubule-mediated mechanical feedback to form flattened leaf blades (20).

PAT is a highly dynamic phenomenon in the shoot apex (12, 14, 21, 22). It remains unknown how PAT around emerging leaf primordia determines auxin convergence and distribution within primordia. It is also unclear how PAT intersects with the expression of leaf patterning genes. In this study, we combined live imaging and microsurgery techniques to show how auxin response output within primordia is determined by PAT in surrounding cells. We also showed how the spatial expression of the leaf shape master regulator is tailored by PAT and auxin distribution. These experimental data are further complemented by computer model simulations which propose how oval auxin distribution pattern emerges and is further maintained during leaf morphogenesis.

Results

PAT around Emerging Leaf Primordia. PIN1-mediated PAT routes in the shoot apex are very dynamic (23, 24) which can be demonstrated by high-resolution imaging technologies (14, 21). Thus, we used high-resolution confocal laser scanning microscopy to analyze the subcellular localization of PIN1 in tomato plants expressing a *pAtPIN1::AtPIN1-GFP* transgene (*SI Appendix*, Fig. S1) (25). In particular, we focused on incipient leaf primordia and emerging early leaf primordia, especially I_1, which denotes the oldest incipient leaf primordium, and P_1, which denotes the youngest visible leaf primordium (Fig. 1). The dynamic PIN1 polarity and derived PAT can be summarized as follows.

  i. There is a primary convergence of PIN1 toward the center of the SAM.
 ii. In I_1 and early P_1, PIN1 converges toward the sites of organ initiation (9, 14).
iii. Additionally, in I_1 and early P_1, some PIN1 proteins between the SAM summit and primordium center point toward two lateral regions of the primordium (Fig. 1 A–E).
 iv. Starting from late P_1, the PIN1 polarity becomes inverted at organ boundaries toward the SAM summit, and convergence at the lateral regions is strengthened (Fig. 1 F and G).
  v. In I_1 and P_1, PIN1 between (incipient) primordia points toward one of the neighboring primordia or toward the SAM summit (Fig. 1 H–J).

These observations expand upon the findings of previous studies (9, 14) and provide interesting insights into PAT dynamics in and the proximity of emerging leaf primordia (Fig. 1Q).

Spatial Auxin Response Output in Leaf Primordia. To quantitatively assess the spatial auxin response output, we next imaged the distribution of the synthetic auxin-induced transcriptional reporter *pDR5::3×Venus-N7* in the shoot apex (26). Surrounding the SAM center, *DR5* is expressed in discrete cell clusters that are in the epidermis and correspond to incipient primordia (Fig. 1 K–M). Starting from I_1, *DR5* extended into the inner cells. In P_1 and P_2, *DR5* is mainly expressed in inner cells, and at the distal tip, including those in the epidermis. Within inner cells, the *DR5* expression region was oval shaped, with the mediolateral axis being longer than the adaxial–abaxial axis.

Weaker *DR5* signals were also found in the adaxial epidermis, especially the lateral marginal regions (Fig. 1 N and O). At P_4, the *DR5* signal was predominantly detected in the provascular tissue, middle domain cells, and epidermal cells in the lateral marginal regions (Fig. 1P). Like in Arabidopsis (11, 12), the *DR5* expression maximum shifts across the adaxial side to the middle domain in tomato. The *DR5* activity decrease on the adaxial side is slightly slower in tomato than in Arabidopsis so that adaxial *DR5* signal remains detectable in P_2 in tomato (Fig. 1O). The auxin response requires class-A ARFs, and *SlMP* is the major ARF in leaf development (19). *SlMP* expression is enriched in the adaxial domain, including the primordium tip in $P_{1–2}$, and is more enriched in the middle domain in later-stage leaves (19). As such, the expression pattern of *SlMP* substantially overlaps with the *DR5* pattern and is similar to that of Arabidopsis *MP* (11).

Overall, PIN1 localization and polarity and auxin response output are very dynamic and interconnected during early leaf development, likely constraining expression domains of master regulators of leaf flattening in tomato (Fig. 1Q). We also tested genetically encoded auxin biosensor DII-Venus that has been used before for reporting endogenous auxin levels in Arabidopsis (27). Nevertheless, we found that DII-Venus barely produced signals in tomato leaf primordia, presumably due to faster reporter degradation in tomato.

Tangential and Lateral Incisions Lead to Similar Redistribution of Auxin Convergence Points. Microsurgical incisions have been efficient in inferring mobile signals in the shoot apex (7, 9, 14). Furthermore, by applying the PAT inhibitor 1-*N*-naphthylphthalamic acid (NPA) locally to mimic incisions, one may test whether PAT serves as a mobile signal in tomato. To understand the contributions of PAT to spatial auxin response output and leaf primordium development, we made incisions on and applied NPA to the abovementioned reporter lines. Two types of incisions/treatments were carried out, with corresponding controls also included (Fig. 2 A–J). A tangential incision was made between the SAM and I_1 (7, 9, 28), and lateral incisions were made on both sides of an I_1 (13, 14). Consistent with previous reports, we observed high frequencies of axisymmetric leaf formation (Fig. 2 I and J).

Tangential incisions were applied at I_1, and leaf primordia were imaged 6 h after incisions. At I_1, the PIN1 polarity points toward the primordium center, and lateral PIN1 convergence points start to form (Fig. 1 B and C). Long tangential incisions, which lead to axisymmetric leaves, caused precocious PIN1 polarity inversion toward the SAM summit and compromised lateral PIN1 convergence point formation along future leaf margins (Fig. 2 K and L). The *DR5* signal substantially decreased after the incision. Importantly, the oval-shaped *DR5* domain was altered along the mediolateral axis, producing more of a symmetrical shape (Fig. 3 A and B). Short tangential incisions, which did not affect leaf development, also led to precocious PIN1 polarity inversion but did not affect the lateral PIN1 convergence points (Fig. 2K). The spatial distribution of the *DR5* signals was comparable to that in normal leaves (Fig. 3A).

After two-sided lateral incisions were made at the I_1 stage, the lateral PIN1 convergence points diminished and became redirected toward the center. In contrast to the tangential incision, PIN1 still pointed toward the primordium tip from the SAM (Fig. 2 M and N). The spatial *DR5* signal distribution became withdrawn from lateral regions and was concentrated toward the center (Fig. 3 C and D), which is similar to the phenomena in response to the tangential incision. Nevertheless, the reduction in *DR5* signal level was less severe after the two-sided lateral incisions
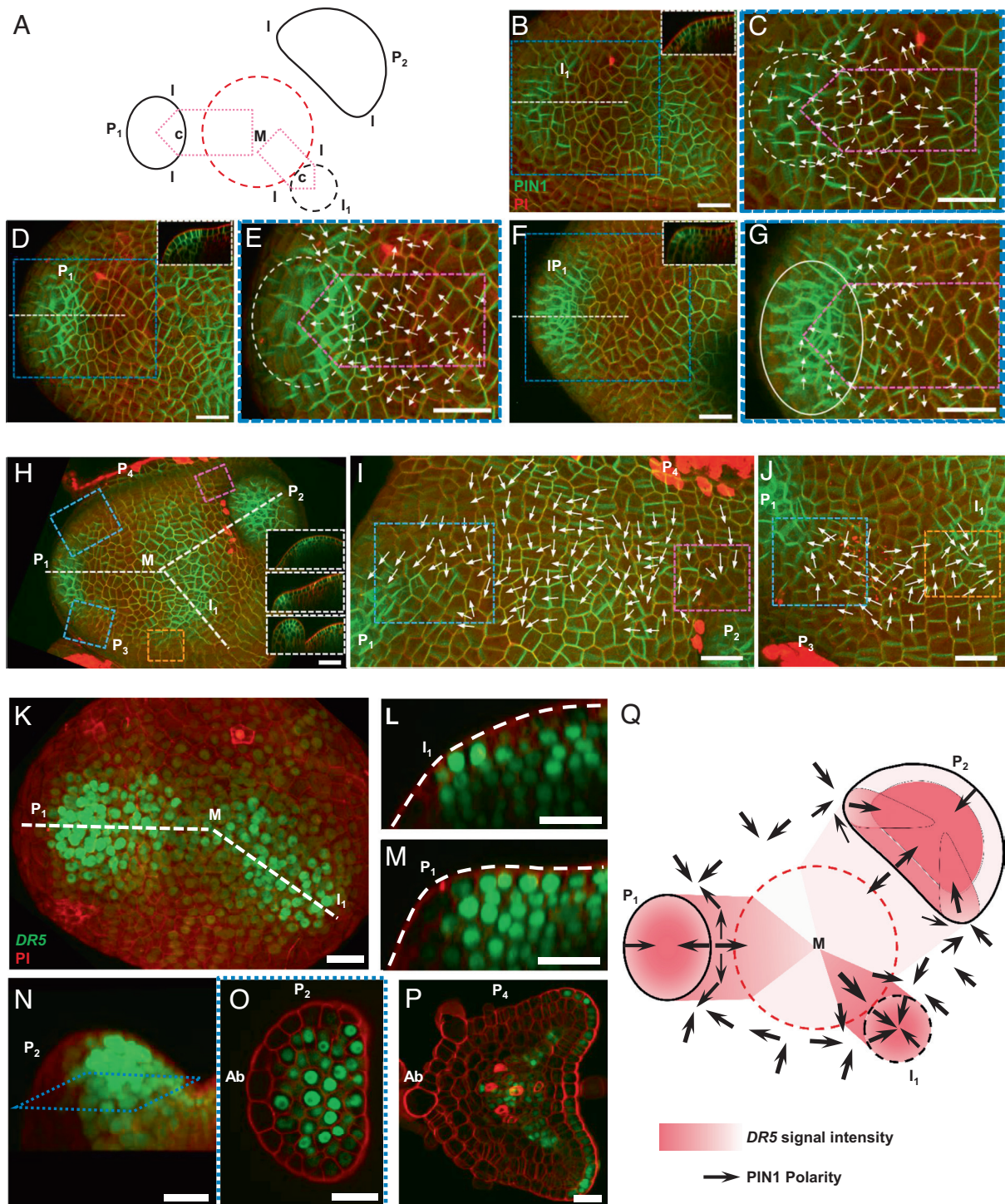
Fig. 1. Spatial distribution of PIN1 and the auxin response in the shoot apex. (*A*) Schematic view of the tomato shoot apex showing the SAM (M), I_1, P_1, and P_2. The central adaxial regions and lateral regions are marked with c and l, respectively. The boxes bordered by the pink dotted lines correspond to those in (*C*), (*E*), and (*G*). I_1 denotes the oldest incipient leaf primordium, and P_1 and P_2 denote the youngest and second youngest visible leaf primordia, respectively. (*B–G*) Top view of regions of tomato shoot apices showing 3D volume renderings of AtPIN1-GFP (green) localization with Propidium Iodide (PI, red) staining. (*B*, *D*, and *F*) show I_1, P_1, and late P_1 (IP_1), respectively. The white dashed lines indicate positions of optical longitudinal sections displayed as inserts. (*C*, *E*, and *G*) The regions in blue rectangle boxes in (*B*), (*D*), and (*F*) were imaged at enhanced resolution to show AtPIN1-GFP polarity (arrows). Examples of polarity inference are shown in *SI Appendix*, Fig. S1. The white ovals in (*C*), (*E*), and (*G*) highlight the leaf primordia. (*H–J*) Shoot apex showing AtPIN1-GFP polarity between (incipient) primordia. (*I* and *J*) are zoomed-in images of (*H*) showing regions between P_1 and P_2, and I_1 and P_1, respectively. The orange, blue, and pink boxes mark the lateral sides of I_1, P_1, and P_2, respectively. (*K–M*) Top view of regions of tomato shoot apices showing 3D volume renderings of *pDR5::3×Venus-N7* (green) expression patterns with PI (red) staining. The white dashed lines in (*K*) indicate positions of optical longitudinal sections in (*L*) and (*M*). (*N* and *O*) 3D volume rendering (*N*) and optical transverse section (*O*) of a P_2 showing DR5 signals. Ab, abaxial domain. (*P*) Cross-section of a P_4 showing DR5 signals. (*Q*) Schematic summary of spatial PIN1 polarity and auxin response output. (Scale bars, 25 μm.)

were made. A single lateral incision at one side did not lead to axisymmetric leaves. We found that a one-sided lateral incision at I_1 affected lateral PIN convergence at the cut side but not the other

side of the leaves (Fig. 2*M*). Spatial *DR5* signal distribution was not strongly affected by one-sided lateral incisions and was similar to that in uncut leaves (Fig. 3*C*). In P_4-stage axisymmetric leaves,
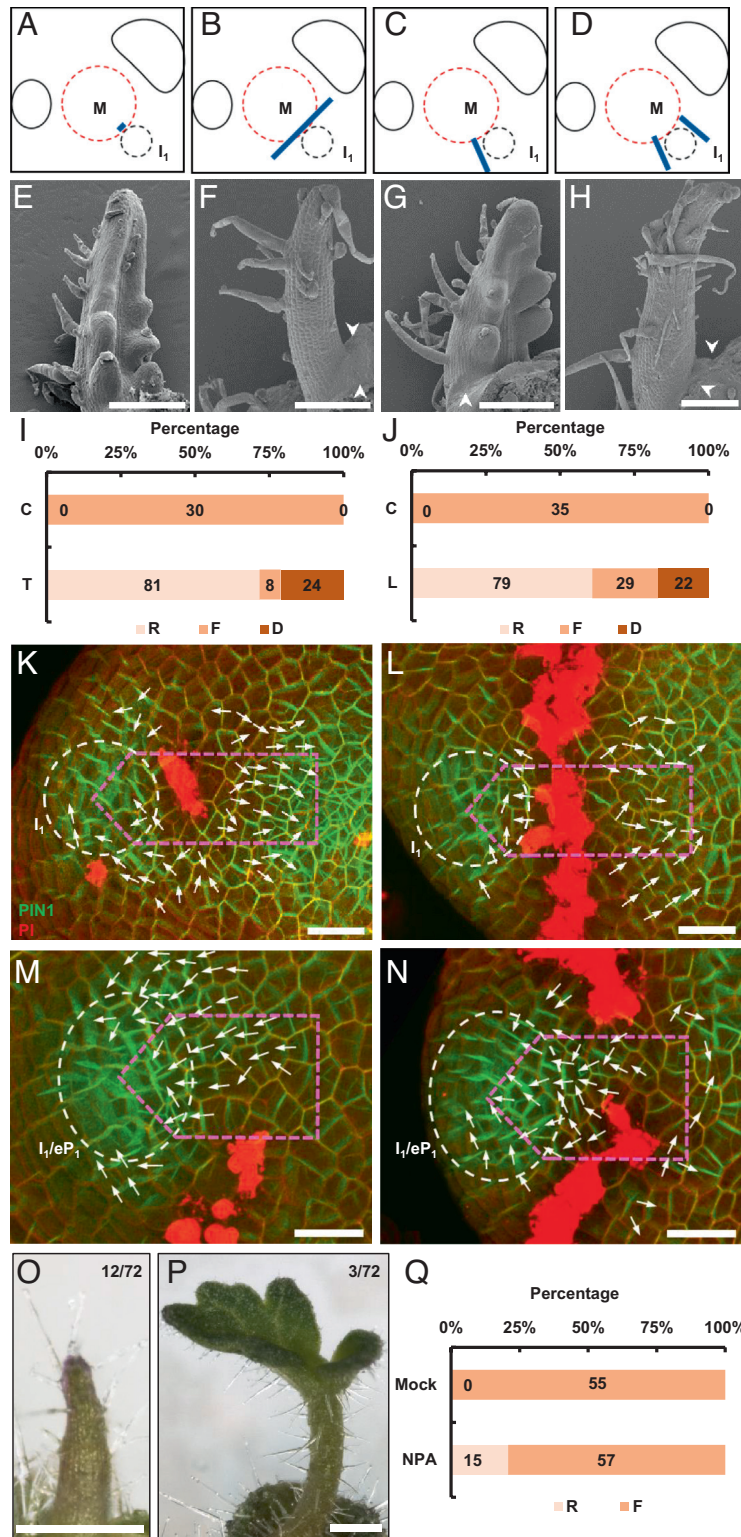
Fig. 2. Microsurgical incisions change the PIN1 polarity field. (A–D) Schematic illustrations of microsurgical incision and controls. (A), control for tangential incisions; (B), tangential incisions; (C), control for lateral incisions; and (D), lateral incisions. The blue lines indicate incisions. (E–H) Representative leaf primordia 5 to 7 d after incisions shown in the corresponding *Upper* panels (A–D). Radially symmetric leaves are shown in (F) and (H). The white arrowheads indicate incisions. (I and J) Quantification of phenotypes obtained 5 to 7 d after control and tangential incisions (I), and after control and lateral incisions (J). R, radially symmetric; F, full blade; D, defective blade. (K–N) Top view of regions of representative tomato shoot apices showing 3D volume renderings of AtPIN1-GFP (green) localization with PI (red) staining 6 h after incisions. (K), (L), (M), and (N) correspond to incisions shown in (A), (B), (C), and (D), respectively. The white ovals highlight the leaf primordia. The boxes bordered by the pink dotted lines indicate the leaf central domain and neighboring SAM regions, as shown in Fig. 1A. The white arrows indicate AtPIN1-GFP polarity. (O–Q) Local NPA-containing lanolin paste lines at positions shown in (D) reproducibly induce radially symmetric leaves (O) and trumpet leaves (P). (Q), Quantifications of phenotypes obtained 7 d after NPA treatment. R, radially symmetric; F, full blade; D, defective blade. [Scale bars, 200 μm in (E–H), 25 μm in (K–N), and 500 μm in (O and P).]
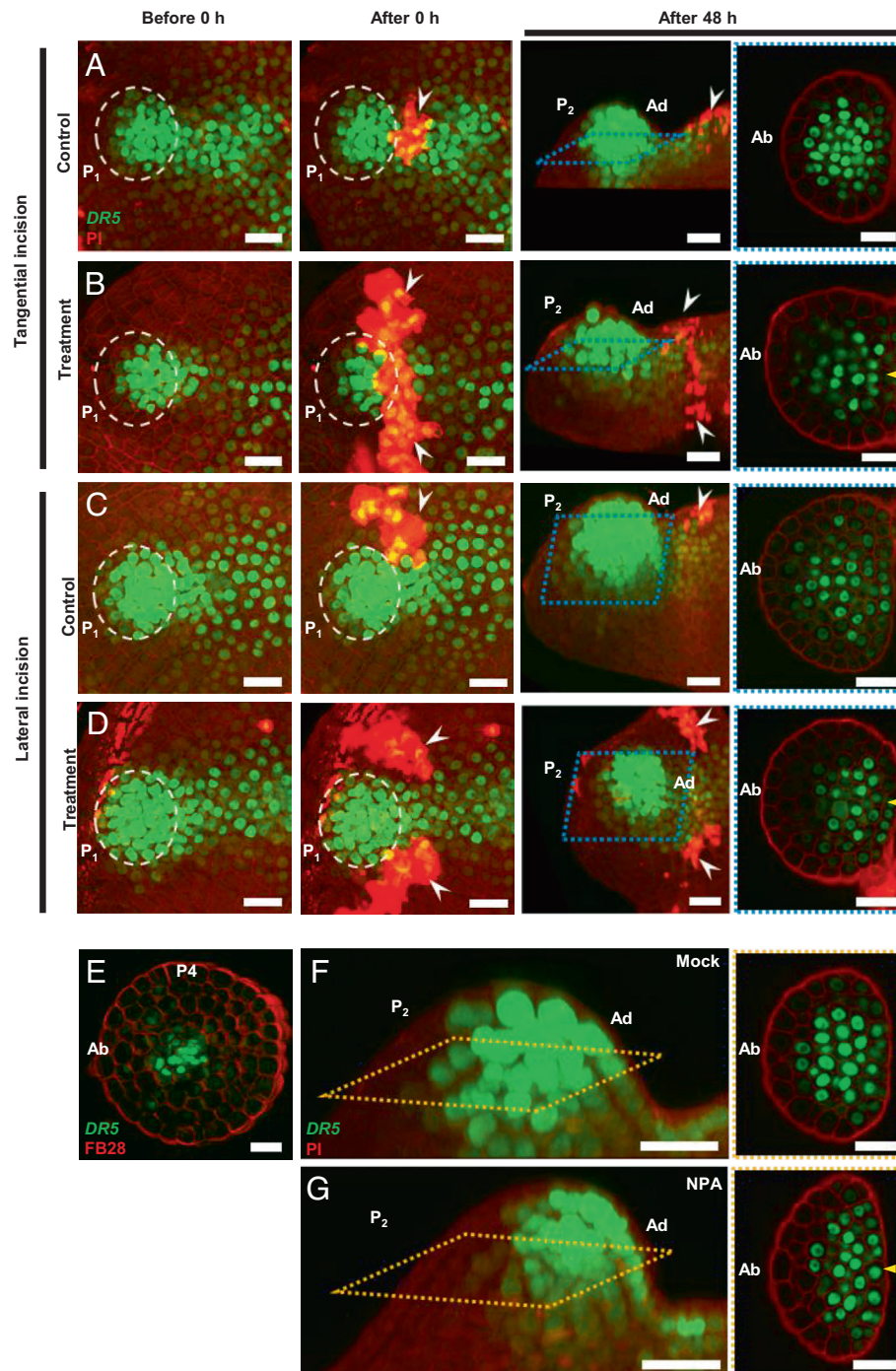
Fig. 3. Microsurgical incisions and NPA treatment alter spatial auxin response output. (*A–D*) Time-lapse images of regions of tomato shoot apices showing 3D volume renderings of *pDR5::3×Venus-N7* (green) expression patterns with PI (red) staining. The white ovals in the first (before incisions) and second (after incisions) columns highlight the leaf primordia. The arrowheads in the second and third (2 d after incisions) columns indicate sites of incisions. The blue boxes in the third column correspond to positions of optical cross-sections shown in the fourth column. (*A–D*) correspond to incisions shown in Fig. 2 *A–D*, and the same primordium is shown for each panel. (*E*) Cross-section of a radially symmetric P_4 2 d after long tangential incisions were made as in (*B*), showing DR5 signals. (*F* and *G*) Regions of tomato P_2 showing 3D volume renderings of *pDR5::3×Venus-N7* (green) expression patterns with PI (red) staining. The organ boxes in the leaf column correspond to positions of optical cross-sections shown in the right column. (*F*), mock lanolin paste; and (*G*), NPA-containing lanolin paste. The lanolin lines were applied at the two lateral sides of I1 primordium as indicated in Fig. 2*D*. Yellow arrowheads in (*B*), (*D*), and (*G*) indicate the enrichment of *DR5* signal in the adaxial region of leaf primordium. Ab, abaxial; Ad, adaxial. (Scale bars, 25 μm.)

the *DR5* signal was centrally localized in provascular tissue and surrounding cells (Fig. 3*E*).

We previously showed that applying lanolin paste-containing NPA in a long tangential line (~20 μm or ~2 cells wide) could mimic a microsurgical incision at the same site (9). To precisely test the roles of PAT in lateral regions, we applied two-sided lateral NPA lines at the I_1 stage, mimicking lateral incisions. After applying NPA lines, we obtained axisymmetric leaves similar to those produced after lateral incisions were made (Fig. 2 *O–Q*). We found that the *DR5* signal distribution was also affected by two-sided lateral NPA lines, similar to that resulting from lateral incisions (Fig. 3 *F* and *G*).

Computer Model of PAT Disturbance Predicts Alternations of Auxin Distribution Patterns. To better understand the dynamics behind PAT and leaf formation, we constructed a computer model that simulates auxin transport, auxin distribution, and downstream master regulator expression across the surface of a tomato apical meristem (Fig. 4A). Our model addresses a possible mechanism underlying PAT activity in the SAM and is compatible with our experimental observations derived from microsurgical incisions, and their effects on final leaf shape. The model uses a digitized cellular mesh obtained from confocal microscopy images of a tomato SAM where cells are represented as polygonized elements (*Materials and Methods*). The computer model integrates auxin active transport through PIN1 as well as subcellular dynamics of PIN1 auxin efflux carriers. Several models of auxin transport in the SAM have been proposed, and a general consensus has led to two main hypotheses: auxin canalization also known as with-the-flux dynamics, or up-the-gradient PIN polarization (29). However, neither of these two mechanisms seems to be capable of completely reproducing the observed auxin distribution across multiple tissues (30). The solution presented in the current model aims to reconcile these two mainstream hypotheses concerning PIN polarization via integration of both ideas to investigate this phenomenon across the surface of the SAM depending on specific conditions (Fig. 4B): (i) in the presence of low auxin concentrations, during which PIN1s polarize preferentially with the flux, therefore reinforcing the current auxin flow direction, and (ii) in the presence of high
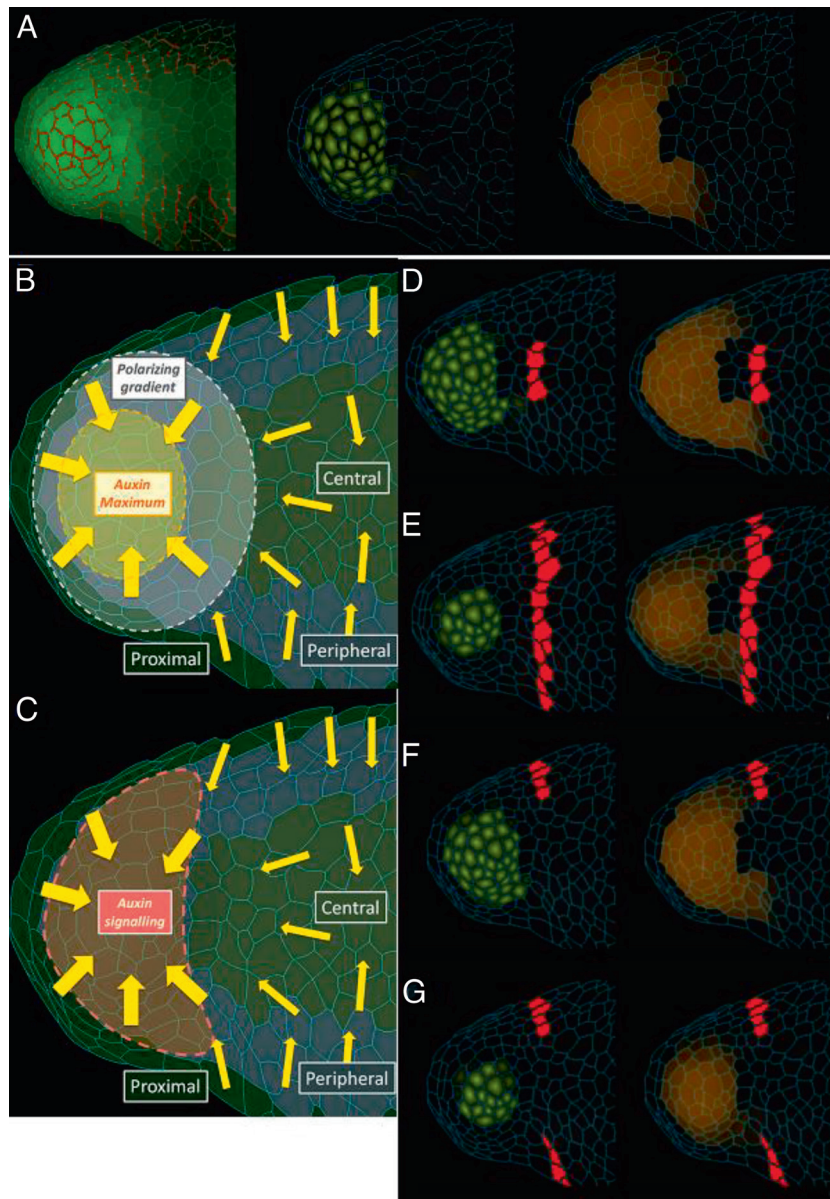

Fig. 4. Computer model simulations recapitulate PAT dynamics required for leaf bilateral symmetry. (*A*) Computer model simulation of PAT across the surface of the tomato apical meristem (see *Materials and Methods* for details). Distribution of auxin concentration in the surface cells of an incipient primordium (green color intensity) and corresponding PIN localization (red color) on the cell membrane (*Left*). Auxin internalization in the inner tissues (*Middle*). Auxin signal distribution in the surface cells (*Right*). (*B*) Model schematic description. The SAM is subdivided into three main zones: peripheral, proximal, and central zones. Auxin is produced only in the proximal and peripheral zones. At low concentrations, auxin polarizes preferentially with the flux. A high auxin concentration activates the expression of a polarizing signal that allows the formation of an auxin maximum over the incipient primordium. (*C*) Auxin signaling response in the incipient primordium. Only the peripheral zone is responsive to auxin. (*D*–*G*) Microsurgical incision simulations, showing the effects of cell ablation on auxin distribution in the inner tissues (*Left*) and on the auxin signaling response in the surface cells (*Right*). These simulations reproduce experimental short tangential incisions (*D*), long tangential incisions (*E*), single lateral incisions (*F*), and double lateral incisions (*G*).

auxin concentrations (such the ones occurring at auxin maxima in primordia), during which the production of a hypothetical PIN1s polarity enhancer is activated, which is allowed to diffuse over the meristem surface and promote PIN1 polarization against the auxin gradient. This mechanism reinforces PIN1 polarization toward the incipient primordium and stabilizes the auxin maximum (Fig. 4B). Auxin and polarizer concentrations additionally contribute to triggering the expression of an instrumental "auxin signaling output" (Fig. 4C), which represents a putative activator of auxin-responsive master regulator involved in acquisition of leaf blade shape. In addition, our model assumes that auxin is produced outside the SAM and in the peripheral zone and not in the central zone (31). We also assumed that only the peripheral zone could generate auxin response as suggested before (11). To set boundary conditions, auxin initially flows from the proximal zone to the central zone because cells belonging to the outermost ring of the proximal zone tend to polarize toward the centroid of the SAM structure. Later, PINs are polarized based on either of the two proposed mechanisms: "up-the-gradient" and "with-the-flow". Next, we tested whether these assumptions are in principle, sufficient to reproduce oval auxin distribution pattern in the SAM and explain the downstream effects of microsurgical incisions observed in experiments.

Our experimental data indicate that the expression of the auxin-responsive synthetic gene *DR5* presents a characteristic oval shape distribution pattern, especially in inner cells (Fig. 1). Notably, the auxin distribution predicted by the model closely matches this experimental *DR5* expression pattern (Fig. 4A), demonstrating that the modeled mechanism is capable of redistributing auxin across the SAM surface (Fig. 4A, *Left*) and generating a stable oval auxin maximum inside the incipient primordium (Fig. 4A, *Middle*). Furthermore, our model could reproduce an auxin signaling pattern that predicts the arc-shaped pattern along the mediolateral axis across the SAM surface of putative downstream regulator of leaf blade shape (Fig. 4A, *Right*). These predictions demonstrate that our model supports experimental observations, highlighting the plausible conditions that could lead to bilateral leaf blade shape in the SAM.

Next, we tested the effects of a virtual incision across the SAM surface to understand the connection between PAT dynamics and auxin response output in leaf primordia (Fig. 4 *D–G*). Microsurgical incisions and cell death were simulated by "disabling" model cells by making the selected cells incapable of transporting and diffusing auxin, as well as by making them unresponsive to any chemical stimulus. We show that a long tangential incision and double lateral incisions have drastic effects on auxin distribution and the auxin response in the incipient primordia (Fig. 4 *E* and *G*). Auxin is substantially reduced, and the distribution pattern of auxin in the inner tissues shifts from the typical oval shape to a more symmetric round shape (Fig. 4 *E* and *G*), as reflected by *DR5* spatial expression patterns seen in our experiments (Fig. 3). Auxin signaling in the epidermis is also significantly reduced, particularly at the extreme end of the arc-shaped distribution pattern (Fig. 4 *E* and *G*). Conversely, a short tangential incision and a single lateral incision that did not produce visible effect of leaf development in the experiment had little impact on auxin levels and signaling (Fig. 4 *D* and *F*). Taken together, our findings provide additional support for the idea that PAT originating from SAM is required for the geometric distribution underlying auxin maxima and thereby the proper response of downstream genes that are involved in the primordium development. Interestingly, similar microsurgical incisions do not affect leaf flattening in Arabidopsis (32). We hypothesize that local auxin biosynthesis observed early during leaf formation in Arabidopsis

(12) could uncouple the primordia from necessity for external auxin supply that is observed in tomato. We tested this idea using a computer model and indeed, we found that auxin biosynthesis could explain why Arabidopsis is less sensitive to incisions as primordia is dominated by up-the-gradient mechanism (*SI Appendix*, Fig. S2).

Alteration of SlLAM1 Spatial Distribution in Response to Microsurgical Incisions. Leaf polarity genes are essential for leaf shape determination. The middle domain marker gene *SlLAM1* is required for blade formation (33, 34). Furthermore, the expression of *SlLAM1* is promoted by auxin (34, 35), which is similar to its homologs in Arabidopsis (11). Using a *pSlLAM1::N7-2×Venus-LhG4* reporter (34), we analyzed the spatial expression changes of *SlLAM1* after tangential and lateral incisions were made.

In untreated leaves or leaves in which a short tangential incision was made, the *SlLAM1* expression pattern formed an arc along the mediolateral axis that covered the leaf primordium middle domain and extended out of the lateral regions at the P₁ stage (*SI Appendix*, Fig. S3 *A–D*), the pattern of which is similar to that of homologous *PRS* expression in Arabidopsis (11, 15, 16). By early P₂, *SlLAM1* expression was stronger in the lateral regions including the leaf margins, but also was weakly detected in the adaxial domain. By P₄, *SlLAM1* expression was restricted to the middle domain, especially the leaf margins (Fig. 5 *A–C*). Therefore, *SlLAM1* expression patterns mirror that of *DR5* spatial expression patterns, although *SlLAM1* exhibited reduced expression in provascular cells.

After long tangential incisions were made, *SlLAM1* expression in the lateral regions was reduced by P₁ (Fig. 5 *D* and *E* and *SI Appendix*, Fig. S3 *A–H*). By early P₂, no expression in the lateral regions was detected, but low expression levels persisted in the center (Fig. 5E). We also made one-sided and two-sided lateral incisions. Although the one-sided lateral incisions did not obviously change the *SlLAM1* expression pattern in P₁ and P₂ (Fig. 5 *F* and *G* and *SI Appendix*, Fig. S3 *I–P*), the two-sided lateral incisions led to a similar reduction in lateral signals. Unlike the long tangential incisions, the two-sided lateral incisions resulted in enhanced adaxial *SlLAM1* signals by early P₂ (Fig. 5G). The expression of *SlLAM1* was no longer detected by P₄ after either long tangential incision or two-sided lateral incisions (Fig. 5H). We also applied two-sided lateral lines of NPA-containing lanolin and detected changes in *SlLAM1* expression patterns very similar to those resulting from two-sided lateral incisions (Fig. 5J). To directly test whether ectopic *SlLAM1* expression in the middle of the adaxial domain is caused by ectopic auxin signaling in the same cells, we locally treated the adaxial domain with lanolin containing the auxin analog 2,4-dichlorophenoxyacetic acid (2,4-D). Adaxial 2,4-D treatment similarly activated ectopic *SlLAM1* expression (Fig. 5 *K–M*).

Overall, *SlLAM1* expression is altered in response to long tangential or two-sided lateral incisions, and the change in spatial expression is similar to that of *DR5*. Initially, laterally enriched *SlLAM1* expression decreased, resulting in reduced *SlLAM1* expression in the center. Later, *SlLAM1* expression disappeared in the leaf primordia. The application of NPA lines resulted in similar changes, reconfirming the roles of PAT in regulating the spatial pattern of *SlLAM1* expression.

Inhibition of SlREV by Incisions. We next sought to determine whether the adaxial and abaxial domains were altered by incisions and auxin signaling. To this end, we generated *pSlREV::mTurquoise2-SlREV* reporters, which are sensitive to Sly-miR166 (36). *SlREV* is targeted by *Sly-miR166*, and we have
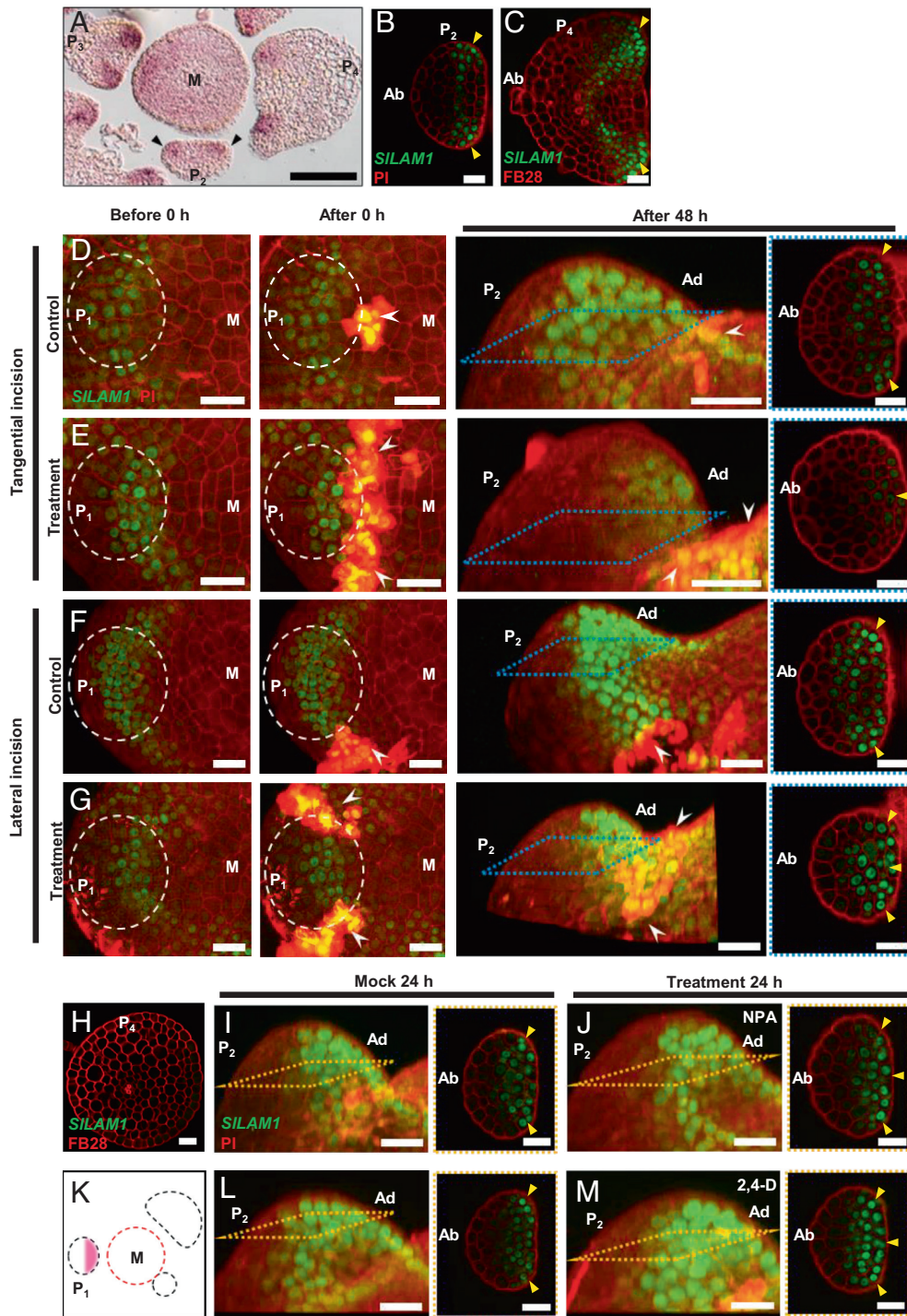
Fig. 5. Microsurgical incisions and NPA treatment alter *SlLAM1* expression patterns. (*A*) ISH of *SlLAM1* mRNA in a transverse section of a wild-type M82 vegetative apex. The arrowheads indicate the enrichment of the *SlLAM1* signal in leaf margins. The probe was used in ref. 34, where a comparable control hybridization using the sense probe was provided. (*B* and *C*) Expression patterns of *pSlLAM1::N7-2×Venus-LhG4* (green) in P₂ and P₄ transverse sections stained with PI or FB28 (red). (*D–G*) Time-lapse images of regions of tomato shoot apices showing 3D volume rendering of *pSlLAM1::N7-2×Venus-LhG4* (green) expression patterns with PI (red) staining. The white ovals in the first (before incisions) and second (after incisions) columns highlight the leaf primordia. The arrowheads in the second and third (2 d after incisions) columns indicate sites of incisions. The blue boxes in the third column correspond to positions of optical cross-sections shown in the fourth column. (*D–G*) correspond to incisions shown in Fig. 2 *A–D*, and the same primordium is shown for each panel. More time points are shown in *SI Appendix*, Fig. S3. (*H*) Cross-section of a radially symmetric P₄ 2 d after long tangential incisions as in (*E*) were made, showing *SlLAM1* signals. (*I* and *J*) Regions of tomato P₂ showing 3D volume renderings of *pSlLAM1::N7-2×Venus-LhG4* (green) expression patterns with PI (red) staining. The orange boxes in the *Left* panel correspond to positions of optical cross-sections shown in the *Right* panel. (*I*), Mock lanolin paste; (*J*), NPA-containing lanolin paste. The lanolin lines were applied at the two lateral sides of I1 primordium as indicated in Fig. 2D. (*K*) Schematic illustration of the application of lanolin paste that included 2,4-D to the P₁ adaxial domain. (*L* and *M*) Regions of tomato P₂ showing 3D volume renderings of *pSlLAM1::N7-2×Venus-LhG4* (green) expression patterns with PI (red) staining. The orange boxes in the *Left* panel correspond to positions of optical cross-sections shown in the *Right* panel. (*L*), Mock lanolin paste; (*M*), lanolin paste including 2,4-D. The lanolin paste was applied as in the same manner as that shown in (*K*). Yellow arrowheads in (*B–G*), (*I*), (*J*), (*L*), and (*M*) indicate the enrichment of *SlLAM1* signal in leaf margin. M, meristem summit; Ab, abaxial; Ad, adaxial. [Scale bars, 100 μm in (*A*); 25 μm in (*B–G*), (*H–J*), (*L*), and (*M*).]

ensured that the *Sly-miR166* target site is unaltered. The expression of the reporters was nearly the same as the endogenous *SlREV* expression determined by in situ hybridization (ISH; Fig. 6*A*). In plants coexpressing both *pSlREV::mTurquoise2-SlREV* and *pSlLAM::N7-2xVenus-LhG4*, we found that *SlREV* was expressed in the SAM center and extended into incipient primordia by I_1. The expression of *SlREV* largely overlapped with that of *SlLAM1* in P_1 and P_2, although no lateral enrichment was observed for *SlREV* (Fig. 6 *B–E*). Together, the expression of *SlREV* is highly comparable to that of Arabidopsis *REV*, including the overlap with that of *SlLAM1/PRS* (10, 15, 16).

We made tangential and lateral incisions on the *pSlRE-quoise2-SlREV* marker line. Long tangential incisions resulted in minimal levels of *SlREV* signals 12 h after incision (Fig. 6 *F* and *G*). Using ISH, we confirmed that *SlREV* expression was no longer detected by P_3 (Fig. 6*K*). Short tangential incisions also resulted in reduced *SlREV* signals in the surrounding cells, but *SlREV* expression within primordia remained largely unaffected (Fig. 6*F*). Similarly, two-sided lateral incisions resulted in significantly reduced *SlREV* signals after 16 h (Fig. 6*I*). One-sided lateral incisions also led to reduced *SlREV* expression, although less dramatically (Fig. 6*H*). Notably, the reduction in *SlREV* expression was symmetric, with a similar reduction detected on the uncut side.

Additionally, we asked whether the abaxial domain marker gene expression remains intact after incisions were made. There are multiple Arabidopsis *KAN1* homologous genes; we selected *SlKAN2C* because it exhibited the strongest expression among the *SlKAN* genes (*SI Appendix*, Fig. S4 *B* and *D*). *SlKAN2C* was detected outside the SAM center prior to primordium formation and was expressed in the abaxial side in early primordia (Fig. 6*L*). After long tangential incisions or two-sided lateral incisions, we found that *SlKAN2C* expression was still detectable throughout the leaf primordia (Fig. 6 *M* and *N*). Together, the *SlKAN2C* expression domain expands at the expense of *SlREV* and *SlLAM1*.

Depletion of SlREV Is Independent of Canonical Auxin Signaling.
We next asked whether the depletion of SlREV caused by incisions was mediated by the canonical auxin response pattern established by PAT as in the case of *SlLAM1*. To this end, we used local NPA and 2,4-D treatment to interfere with mTurquoise2-SlREV signals. After applying two-sided lateral NPA-containing lanolin lines, we found that mTurquoise2-SlREV expression was reduced after 24 h but was less affected than that resulting from actual incisions (Fig. 6 *O–R, W*). We also applied 2,4-D-containing lanolin paste to the adaxial side. Surprisingly, we found that the mTurquoise2-SlREV expression pattern was largely unchanged after 24 h, although there was a slight increase in expression (Fig. 6 *S–V, X*). Although the mTurquoise2-SlREV signal was largely unaffected by the auxin response within 24 h, the signal was undetectable after 7 d (Fig. 6 *R* and *V*).

The fast elimination of mTurquoise2-SlREV by incision implies possible proteasome-mediated protein degradation mechanism. To test this theory, we applied MG132, a proteasome inhibitor, immediately after long tangential incisions were made and monitored mTurquoise2-SlREV signals after 12 h. We found that the decrease of mTurquoise2-SlREV protein was clearly attenuated by MG132 (Fig. 6 *Y* and *Z*). Together, surgical incision could lead to fast proteasome-mediated degradation of SlREV, which occurred independently of canonical auxin signaling, and thus complements auxin-regulated *SlLAM1* expression in the generation of leaf blade shape.

Discussion

Leaf Margin Auxin Signaling and *SlLAM1* Expression Depend on PAT. Leaf blade formation is of enormous importance and has

been extensively studied. Recent molecular studies have shown that leaf primordia display prepatterning by adaxial- and abaxial-promoting genes, and the adaxial–abaxial interface is established several plastochrons before primordium emergence (12, 15–17). Afterward, PAT and spatial auxin response output have pivotal roles in the formation of a flattened leaf blade (9, 11). However, how PAT establishes spatial auxin distribution and signaling remains largely unknown. This has been hindered by the highly dynamic growth and PAT pattern changes in the shoot apex. In this study, we employed multiple reporter lines for PAT, auxin response output, and leaf domains to investigate how PAT disturbances lead to the spatial auxin response and constrained *SlLAM1* expression pattern. Importantly, our results show that PAT in the shoot apex leads to PIN1 convergence at the lateral regions starting from I_1 (Figs. 1, 3, and 7), which subsequently activates the auxin response and *SlLAM1* expression in the middle domain and lateral regions (Figs. 5 and 7). This arc-shaped *SlLAM1* expression pattern is essential for blade formation, as it establishes the leaf margins and, thus, bilateral symmetry. PAT in the shoot apex can generate these convergence patterns, as predicted by the computer model simulations (Fig. 4 *A–C*). A mechanical feedback further amplifies the bilateral symmetry along the mediolateral axis to form a flattened blade (20).

In this study, we employed a commonly used AtPIN1-GFP reporter, which showed undistinguishable localization pattern from endogenous SlPIN1 (Solyc03g118740) in the shoot apices (25). In addition to SlPIN1, there are two Sisters of PIN1 (SoPIN1) proteins in tomato, SlSoPIN1a (Solyc10g078370) and SlSoPIN1b (Solyc10g080880), with redundant function to SlPIN1 38. Mutants of SlSoPIN1a have been characterized, in which phyllotaxis and compound leaf development are affected. Nevertheless, no triple PIN mutants have been reported so far in tomato. In Arabidopsis, *pin1* mutants have leaf polarity defects at a low frequency, which is substantially enhanced when combined with *rev* alleles (9), supporting the roles of PAT in leaf flattening.

Microsurgery Blocks Auxin Accumulation toward Leaf Margins.
Microsurgical experiments by Sussex and others remain the cornerstone of this field (4, 5). We further analyzed how auxin response output and leaf polarity genes could be affected by incisions or local PAT inhibition (Fig. 3 *F* and *G*). We found that such perturbations specifically eliminate lateral PIN1 convergence points that correspond to future leaf margins (Figs. 4 and 7). This change leads to not only a reduction in auxin response output and *SlLAM1* expression but also shrinkage of the corresponding domains such that they change from being arc shaped to rounded (Figs. 3, 5, and 7). This idea is further supported by model simulations (Fig. 4 *D–F*). A change in the *WOX* domain shape leads to a more axisymmetric primordium shape (11), and mechanical feedback maintains axisymmetry to form rod-shaped leaves (20). A recent study in Arabidopsis found that laser ablation of leaf margins on both sides could abolish blade formation (32), supporting the importance of initial bilateral symmetry in leaf flattening. The same study also found that tangential incision or lateral incisions made outside the primordia did not affect blade formation, suggesting that early leaf development in Arabidopsis differs from that in tomato and potato. Notably, our computer model simulations suggest that the timing of auxin production in primordium might be a key factor affecting the sensitivity of primordium to PAT perturbation.

Destabilized SlREV by Wounding May Enhance Flattening Defects. The idea of wounding is often raised as a caveat in the
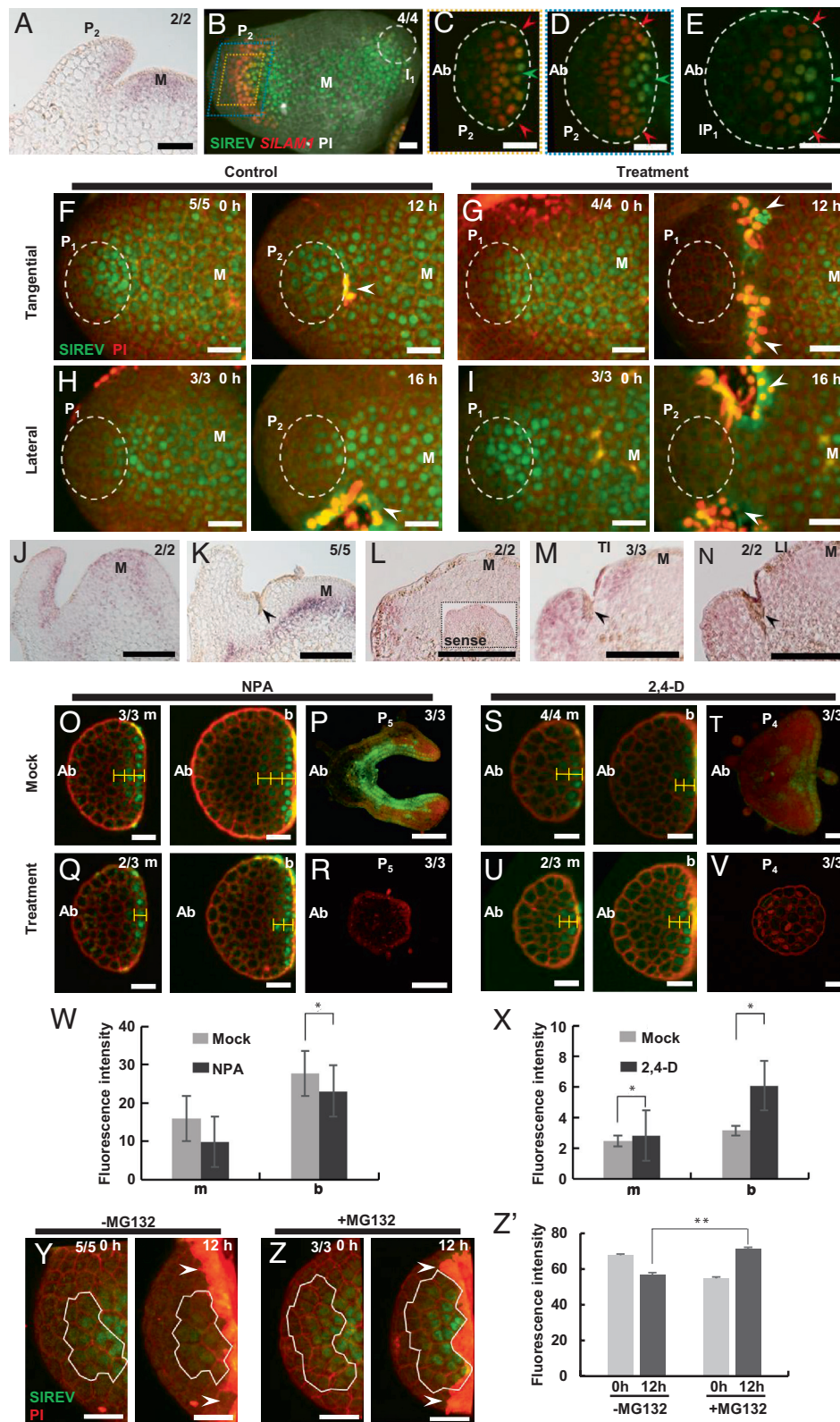
Fig. 6. Microsurgical incisions, NPA treatment, and auxin treatment alter *SlREV* and *SlKAN2C* expression patterns. (*A*) ISH of *SlREV* mRNA in a longitudinal section of wild-type M82 vegetative apex. The probe was used in ref. 37, where a comparable control hybridization using the sense probe was provided. (*B*–*E*) Expression pattern of *pSlREV::mTurquoise2-SlREV* (green) and *pSlLAM1::N7-2×Venus-LhG4* (red). (*B*) Top view of regions of tomato shoot apices showing 3D volume rendering with PI stain (white). The orange and blue boxes correspond to positions of optical transverse sections displayed in (*C*) and (*D*), respectively. (*E*) Independent late P_1 transverse section. The red and green arrowheads highlight the positions of the leaf margin and adaxial domain center, respectively. (*F*–*I*) Time-lapse images of regions of tomato shoot apices showing 3D volume renderings of *pSlREV::mTurquoise2-SlREV* (green) expression patterns with PI (red) staining. *Left*, before incisions; *Right*, 12 h after incision. The white ovals highlight the leaf primordia. The arrowheads in the *Right* panels indicate sites of incisions. (*F*–*I*) correspond to incisions shown in Fig. 2 *A*–*D*, and the same primordium is shown for each experiment. (*J* and *K*) ISH of *SlREV* mRNA in a longitudinal section without (*J*) or 2 d after tangential incisions (*K*), as shown in Fig. 2*B*. (*L*–*N*) ISH of *SlKAN2C* mRNA in a longitudinal section without (*L*), 2 d after tangential incisions (*M*), as shown in Fig. 2*B*, and 2 d after lateral incisions (*N*), as shown in Fig. 2*D*. The *Inset* indicates the result of the sense probe. (*O*–*V*) Transverse sections showing mTurquoise2-SlREV signals after mock (*O* and *P*) and NPA-containing (*Q* and *R*) lanolin applications, as shown in Fig. 2*D*, and mock (*S* and *T*) and 2,4-D-containing (*U* and *V*) lanolin
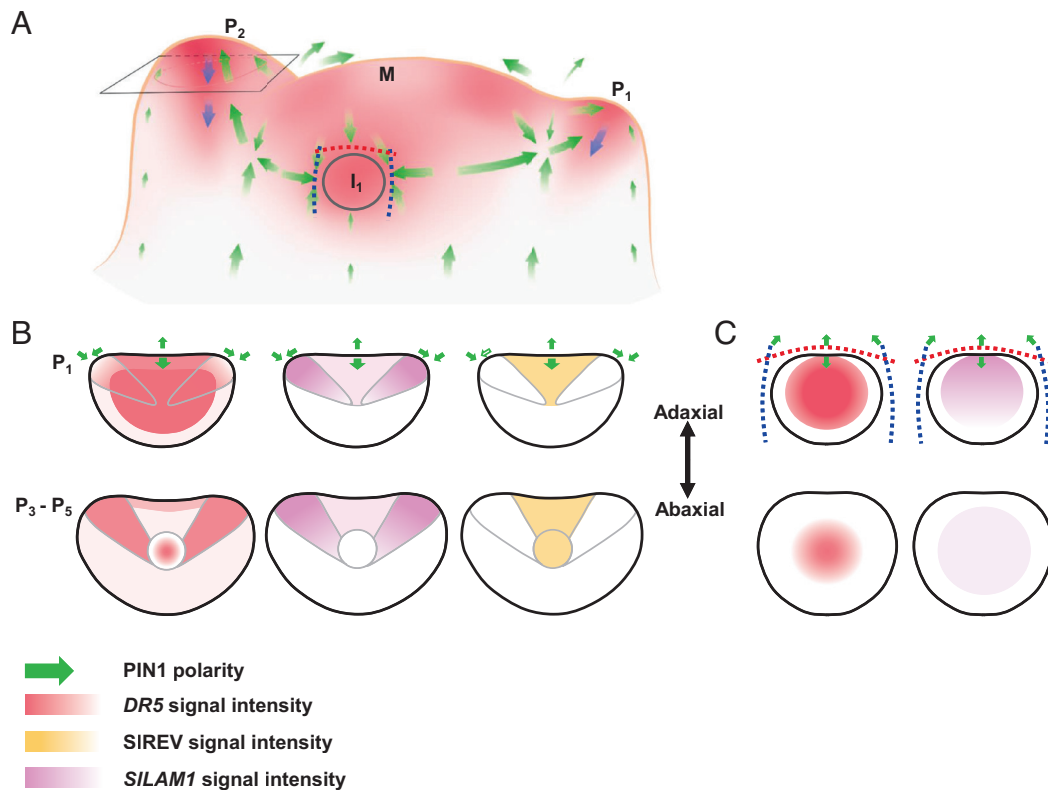
Fig. 7. Schematic representation of DR5 signal and *SlLAM1* expression in untreated leaves and after incisions or local PAT inhibition. (*A*) Summary of auxin response levels, as reflected by the strength of red color, in the shoot apex. Green and blue arrows show PIN1-mediated PAT direction and strength in the epidermis and inner cells of the primordium, respectively. The microsurgical tangential incision or chemical-containing lanolin paste treatment position was shown as a red dotted line. The microsurgical lateral incisions or chemical-containing lanolin paste treatment positions were shown as dark blue dotted lines. M, meristem. I_1, P_1, and P_2 indicated leaf primordium in different developmental stages. (*B* and *C*) Spatial auxin response output and *SlLAM1*, SlREV signal patterns in untreated leaf primordia (*B*) and primordia after microsurgical incisions or chemical treatments (*C*). The expression of SlREV largely overlapped with that of *SlLAM1* in P_1, and P_2 except the lateral regions in untreated plants. Both *DR5* signal and *SlLAM1* expression domains are oval shaped in untreated plants but become more symmetric round shaped after incisions or local PAT inhibition. SlREV signal was more strongly reduced after incisions than after local PAT inhibition.

Sussex experiment (13, 16). In particular, wounding has been proposed to induce auxin depletion and activate *KAN1* expression. However, extensive control experiments performed by Sussex and others suggest that wounding alone is insufficient to trigger leaf patterning defects (5). Here, we show that wounding indeed causes fast degradation of SlREV, which is largely independent of auxin and is mediated by the 26S proteasome pathway. Fast degradation of mTurquoise2-SlREV was not detected after NPA lines or 2,4-D was applied (Fig. 6 *Y, Z*), although mTurquoise2-SlREV still continued to decrease after 7 d. Given that NPA and 2,4-D also induced the formation of axisymmetric leaves, wounding is not necessary for leaf patterning but may increase the frequency of the phenotype. In contrast, manipulating auxin alone is sufficient to obtain changes in polarity gene expression patterns comparable to those obtained in response to surgical incisions.

By connecting high-resolution details of PAT with polarity gene expression during early leaf development, this study shows that the formation of oval-shaped auxin patterns within leaf primordium is essential for leaf flattening. This finding not only answers a long-standing question in developmental biology, but also sheds light on the modulation of leaf shape in tomato, potato, and other related Solanaceae species. The levels of leaf flattening can influence blade size, which positively enhances photosynthesis and negatively affects draught resistance. Our study suggests that fine-tuning PAT in leaf primordium may optimize leaf size to better adapt to changing environments.

Materials and Methods

Tomato (*Solanum lycopersicum*) cultivar M82 was used as the wild type unless otherwise specified. Tomato plants were grown in 1/2-strength Murashige and Skoog media at 25 °C under the long-day condition (16 h light/8 h darkness) for approximately 1 wk until the third or fourth plastochron. Details on the following are available in *SI Appendix, SI Materials and Methods*: growth conditions, genetic materials and construction of transgenic plants, microsurgery and laser ablations, chemical treatment, confocal microscopy, image processing, optical microscopy and scanning electron microscopy, RT-PCR, ISH, phylogenetic tree reconstruction, and computational model description. The primers used in this study are listed in *SI Appendix*, Table S1. The tomato gene IDs are listed in *SI Appendix*, Table S2. Model parameter values are listed in *SI Appendix*, Table S3.

---

applications, as shown in Fig. 5*K*. (*O, Q, S, U*) P_2 stage leaves 24 h after treatment, with the *Left* panels showing the middle region and the *Right* panels showing the basal region of leaf primordia. (*P* and *R*) P_5 stage leaves 7 d after treatment. (*T* and *V*) P_4 stage leaves 7 d after treatment. (*W* and *X*) Fluorescence intensity quantification of optical sections for (*O, Q*) and (*S, U*), respectively. *$P < 0.05$. (*Y* and *Z*) Time-lapse images showing mTurquoise2-SlREV signals after tangential sections as shown in Fig. 2*D* with mock (*Y*) and MG132 (*Z*) treatment. *Left*, before incisions; *Right*, 12 h after incisions. The white lines highlight SlREV-positive cells. The white arrowheads indicate incisions. (*Z'*) Fluorescence intensity quantification of optical sections for (*Y*) and (*Z*). **$P < 0.01$. M, meristem summit; Ab, abaxial; [Scale bars, 100 μm in (*A*) and (*J–N*); 25 μm in (*B–I*), (*O*), (*P*), (*R–U*), and (*W–Z*).]

Author affiliations: [a]State Key Laboratory of Plant Genomics and National Center for Plant Gene Research (Beijing), Institute of Genetics and Developmental Biology, The Innovative Academy of Seed Design, Chinese Academy of Sciences, Beijing 100101, China; [b]College of Advanced Agricultural Sciences, University of Chinese Academy of Sciences, Beijing 100049, China; [c]Centro de Biotecnología y Genómica de Plantas (CBGP), Universidad Politécnica de Madrid (UPM), Centro Nacional Instituto de Investigación y Tecnología Agraria y Alimentaria (INIA, CSIC), Campus de Montegancedo, Pozuelo de Alarcón, 28223, Madrid, Spain; [d]State Key Laboratory of Protein and Plant Gene Research, School of Life Sciences, Peking-Tsinghua Center for Life Sciences, Center for Quantitative Biology, Peking University, Beijing 100871, China; and [e]Peking University Institute of Advanced Agricultural Sciences, Shandong Laboratory of Advanced Agricultural Sciences at Weifang, Weifang, Shandong 261000, China

1. A. Maugarny-Cales, P. Laufs, Getting leaves into shape: A molecular, cellular, environmental and evolutionary view. *Development* **145**, dev161646 (2018).
2. F. Du, C. Guan, Y. Jiao, Molecular mechanisms of leaf morphogenesis. *Mol. Plant* **11**, 1117–1134 (2018).
3. P. A. Conklin, J. Strable, S. Li, M. J. Scanlon, On the mechanisms of development in monocot and eudicot leaves. *New Phytol.* **221**, 706–724 (2019).
4. J. Dong, H. Huang, Auxin polar transport flanking incipient primordium initiates leaf adaxial-abaxial polarity patterning. *J. Integr. Plant Biol.* **60**, 455–464 (2018).
5. C. Kuhlemeier, M. C. P. Timmermans, The Sussex signal: Insights into leaf dorsiventrality. *Development* **143**, 3230–3237 (2016).
6. I. M. Sussex, Experiments on the cause of dorsiventrality in leaves. *Nature* **167**, 651–652 (1951).
7. D. Reinhardt, M. Frenz, T. Mandel, C. Kuhlemeier, Microsurgical and laser ablation analysis of leaf positioning and dorsoventral patterning in tomato. *Development* **132**, 15–26 (2005).
8. R. Waites, A. Hudson, *phantastica*: A gene required for dorsoventrality of leaves in *Antirrhinum majus*. *Development* **121**, 2143–2154 (1995).
9. J. Qi *et al.*, Auxin depletion from leaf primordia contributes to organ patterning. *Proc. Natl. Acad. Sci. U.S.A.* **111**, 18769–18774 (2014).
10. C. Guan, F. Du, Y. Xiong, Y. Jiao, The *35S* promoter-driven mDII auxin control sensor is uniformly distributed in leaf primordia. *J. Integr. Plant Biol.* **61**, 1114–1120 (2019).
11. C. Guan *et al.*, Spatial auxin signaling controls leaf flattening in *Arabidopsis*. *Curr. Biol.* **27**, 2940–2950 (2017).
12. A. Burian *et al.*, Specification of leaf dorsiventrality via a prepatterned binary readout of a uniform auxin input. *Nat. Plants* **8**, 269–280 (2022).
13. R. Snow, M. Snow, Experiments on the cause of dorsiventrality in leaves. *Nature* **173**, 644–645 (1954).
14. J. Shi *et al.*, Model for the role of auxin polar transport in patterning of the leaf adaxial-abaxial axis. *Plant J.* **92**, 469–480 (2017).
15. T. Yu *et al.*, Dynamic patterns of gene expression during leaf initiation. *J. Genet. Genomics* **44**, 599–601 (2017).
16. M. P. Caggiano *et al.*, Cell type boundaries organize plant development. *eLife* **6**, e27421 (2017).
17. A. Y. Husbands, D. H. Chitwood, Y. Plavskin, M. C. Timmermans, Signals and prepatterns: New insights into organ polarity in plants. *Genes. Dev.* **23**, 1986–1997 (2009).
18. D. S. Skopelitis, A. H. Benkovics, A. Y. Husbands, M. C. P. Timmermans, Boundary formation through a direct threshold-based readout of mobile small RNA gradients. *Dev. Cell* **43**, 265–273 (2017).
19. A. Israeli *et al.*, Multiple auxin-response regulators enable stability and variability in leaf development. *Curr. Biol.* **29**, 1746–1759 (2019).
20. F. Zhao *et al.*, Microtubule-mediated wall anisotropy contributes to leaf blade flattening. *Curr. Biol.* **30**, 3972–3985 (2020).
21. C. S. Galvan-Ampudia *et al.*, Temporal integration of auxin information for the regulation of patterning. *eLife* **9**, e55832 (2020).
22. C. Guan, Y. Jiao, Interplay between the shoot apical meristem and lateral organs. *aBIOTECH* **1**, 178–184 (2020).
23. M. G. Heisler *et al.*, Patterns of auxin transport and gene expression during primordium development revealed by live imaging of the *Arabidopsis* inflorescence meristem. *Curr. Biol.* **15**, 1899–1911 (2005).
24. D. Reinhardt *et al.*, Regulation of phyllotaxis by polar auxin transport. *Nature* **426**, 255–260 (2003).
25. E. M. Bayer *et al.*, Integration of transport-based models for phyllotaxis and midvein formation. *Genes. Dev.* **23**, 373–384 (2009).
26. E. Shani *et al.*, Cytokinin regulates compound leaf development in tomato. *Plant Cell* **22**, 3206–3217 (2010).
27. T. Vernoux *et al.*, The auxin signalling network translates dynamic input into robust patterning at the shoot apex. *Mol. Syst. Biol.* **7**, 508 (2011).
28. I. M. Sussex, Experiments on the cause of dorsiventrality in leaves. *Nature* **174**, 351–352 (1954).
29. K. van Berkel, R. J. de Boer, B. Scheres, K. ten Tusscher, Polar auxin transport: Models and mechanisms. *Development* **140**, 2253–2268 (2013).
30. R. S. Smith, E. M. Bayer, Auxin transport-feedback models of patterning in plants. *Plant Cell Environ.* **32**, 1258–1271 (2009).
31. T. Vernoux, F. Besnard, J. Traas, Auxin at the shoot apical meristem. *Cold Spring Harb. Perspect. Biol.* **2**, a001487 (2010).
32. F. Zhao, J. Traas, Stable establishment of organ polarity occurs several plastochrons before primordium outgrowth in Arabidopsis. *Development* **148**, dev.198820 (2021).
33. C. Wang *et al.*, The WOX family transcriptional regulator SlLAM1 controls compound leaf and floral organ development in *Solanum lycopersicum*. *J. Exp. Bot.* **72**, 1822–1835 (2021).
34. F. Du *et al.*, Leaflet initiation and blade expansion are separable in compound leaf development. *Plant J.* **104**, 1073–1087 (2020).
35. A. Israeli, J. W. Reed, N. Ori, Genetic dissection of the auxin response network. *Nat. Plants* **6**, 1082–1090 (2020).
36. V. Omidvar, I. Mohorianu, T. Dalmay, M. Fellner, Identification of miRNAs with potential roles in regulation of anther development and male-sterility in *7B–1* male-sterile tomato mutant. *BMC Genomics* **16**, 878 (2015).
37. J. Qi *et al.*, Mechanical regulation of organ asymmetry in leaves. *Nat. Plants* **3**, 724–733 (2017).
38. C. C. Martinez, D. Koenig, D. H. Chitwood, N. R. Sinha, A sister of PIN1 gene in tomato (Solanum lycopersicum) defines leaf and flower organ initiation patterns by maintaining epidermal auxin flux. *Dev. Biol.* **419**, 85–98 (2016).